Investigation of the Performance of Optical Ray Tracing Simulation in Demonstration of Spherical Aberration

Tongnian Wang

***Abstract*—Inspired by the advances in optics and their contributions to scientific development, this investigation was undertaken to examine the interaction between light rays and optical elements. A simulation was constructed to model and optimize ray optics, and corresponding aberrations. The simulation was able to model ray optics to a high degree of accuracy, with a $3.4 \cdot 10^{-8}\%$ error in modelling ray optics without aberrations. An investigation into spherical aberrations accentuated the limitations of a ray optics simulation with a magnitude extent systematic error. The relationship between transverse and longitudinal spherical aberration was modelled to a high accuracy with 1.5% error from the true value.**

I. Introduction

ADVANCES in optical instruments have driven scientific discovery and breakthroughs in human knowledge. The study of geometric optics originated in the 10th AD with Euclid's Optics. The field was revolutionised in 1604 with Kepler's investigation of ray optics and optical elements in *Astronomiae Pars Optica* [**1**]. The development in astronomy has had a significant dependency on optics and the capability of optical instruments. Aberrations are an observable phenomenon of ray optics, affecting the results of astronomical investigations. Historically, the Hubble telescope suffered from detrimental focusing problems with exaggerated aberrations, which led to images with low quality [**2**].

The project aimed to create a simulation to model the geometrical behaviour of ray optics, neglecting the wave nature of light rays. The investigation of spherical aberration was then carried out utilising the simulation to find an optimised lens system for image formation at a defined distance. The accuracy of the simulation and the success of optimisation has been investigated.

II. Theory

A. Three Dimensional Snell's Law

For this investigation, Snell's law was extended to three dimensions for the completeness of this simulation. Geometrically, the relationship between the incident and refracted ray is expressed by Eq.1 [**3**].

$$(\vec{n} \times \vec{t}) = \mu(\vec{n} \times \vec{i}) \tag{1}$$

Where μ is $n1/n2$. $n1$ is the refractive index of the incident side and $n2$ is the refractive index of the refraction side. $\vec{i}$ is the direction vector of the incident ray and $\vec{t}$ is the direction vector of the refracted ray, $\vec{n}$ is the surface normal vector.

Decompose the two direction vectors into orthogonal vectors parallel and perpendicular to the surface-normal vector. Through algebraic manipulation, $\vec{t}$ is expressed by the function below [**3**].

$$\vec{t} = \vec{n}\sqrt{1 - \mu^2[1 - (\vec{n} \cdot \vec{i})^2]} + \mu[\vec{i} - (\vec{n} \cdot \vec{i})\vec{n}] \tag{2}$$

B. Spherical Aberration

Spherical aberration is the physical phenomenon when rays do not converge to one point after passing through a spherical refracting surface, one of the *'Five Aberrations of Von Seidel'*[**4**]. The further the rays are from the optical axis, the further away they intersect the axis from the paraxial focal point, creating longitudinal and transverse spherical aberration [**5**]. Longitudinal spherical aberration measures the range intersection of rays with the principal optical axis, it is defined in Eq.3 in Coddington notation [**6**]:

$$LSA = \frac{1}{8n(n-1)} \cdot \frac{h^2 i^2}{f^3}[\frac{n+2}{n-1}s^2 + 2(2n+2)sp + (3n+2)(n-1)^2p^2 + \frac{n^3}{n-1}] \tag{3}$$

$$TSA = \frac{h}{i}LSA \tag{4}$$

Where

$$S = \frac{R_2 + R_1}{R_2 - R_1}, \quad p = \frac{i - o}{i + o} \tag{5}$$

Where n is the lens' refractive index, o is the object distance, i is the image distance, h is the distance from the optical axis at which the outermost ray enters the lens, R_1 and R_2 are the respective lens radii, and f is the lens' focal length.

III. Methodology

The simulation used object-oriented programming to model the behaviour of elements of a ray optical system. Including consideration of the attributes and methods of optical elements such as rays and refracting surfaces [**7**].

Optimisation was carries out to deduce the parameters of refracting surfaces which outputs an image with minimum aberration effects at a defined distance. The minimize function from scipy.optimize package was utilised. The relevant parameters of optimization were identified: the thickness of the lens and curvature of the two refracting surfaces. A function was written which takes a tuple as an input, containing the parameters of optimization, and returns the root mean square

spot radius at a defined distance. The function was altered to deduce an optimised plano-convex system; hence the only parameters of optimisation were thickness and the curvature of the anterior surface. Using different methods of minimisation, different combinations of refracting surfaces were deduced through iteration techniques dependent on the method chosen.

IV. Results and Analysis

A. Simulation Accuracy

The theoretical paraxial focal length is $66.67mm$ for a spherical lens with a curvature of $0.03mm$ and a refractive index of 1.5. By propagating a ray along the optical axis with a small displacement in the x-direction, it will experience a minimal extent of spherical aberration. The ray intersected the optical axis $2.25 \cdot 10^{-6}mm$ away from the theoretical paraxial focal point, yielding a 3.375% deviation from the true value. The performance of the optical ray simulation with refracting surfaces is highly accurate when spherical aberration effects are not considered. The Root Mean Square Spot Radius (abbreviated as RMS) for a plano-convex lens at the paraxial focal plane with varying incident beam diameter was measured for both orientations of the lens. From the simulation data (Table I), it is evident that as the diameter of the incident beam increased, the RMS increased. Both relationships are accurately modelled by quadratics, with near identical coefficients, as characterised by the closeness of two lines in Fig.6.

TABLE I
TABLE DEMONSTRATING THE RELATIONSHIP BETWEEN THE DIAMETER OF THE INCIDENT BEAM AND SPHERICAL ABERRATION.

Diameter / mm	RMS_p / μm	RMS_c/ μm
1	6.24	6.09
2	3.78	3.69
4	70.13	68.41
6	261.45	255.11
8	895.12	874.10
10	1225.99	1197.59

RMS_p (posterior refracting surface is convex) was greater than RMS_c (anterior refracting surface is convex) up to the limit when $x \leq 25mm$; relationship was approximated by an exponential relationship. Beyond the limit, the difference decreased sharply and the relationship is reversed.

B. Spherical Aberration of Optimized Lens

Where both the curvatures were optimisation parameters, the majority of the optimised lens systems were plano-convex lenses with a convex anterior surface. Hence, further investigation was taken to find the optimised curvature of the convex surface of a plano-convex lens. The results of different optimisation methods are seen in Table II, where T is the thickness of the lens. Longitudinal spherical aberration (LSA) and transverse spherical aberrations (TSA) are aberrations parallel and perpendicular to the optical axis at the paraxial focal plane respectively. The RMS calculated in Table II is the radius of the circle of least confusion - the location of minimum TSA [**8**].

TABLE II
TABLE CONTAINING OPTIMISED PARAMETERS FOR A PLANO-CONVEX LENS AND RELATED ABERRATION RESULTS.

Method	T/mm	C_1/mm	RMS	TSA	LSA
Nelder-Mead	9.999	0.028	0.008	0.043	0.899
CG	1.000	0.029	0.009	0.048	0.963
L-BFGS-B	1.001	0.029	0.009	0.048	0.963
TNC	5.019	0.028	0.009	0.046	0.934
SLSQP	0.989	0.02941	0.009	0.048	0.964

The mean curvature of the optimised anterior surface was $0.02902 \pm 0.0005mm$. The low uncertainty demonstrated a high level of consistency in the optimisation of a plano-convex lens system in image formation with different minimization methods. The circle of least confusion was positioned at z = $200.00mm$, whereas its paraxial focal point is at $199.39mm$. The expected h/i ratio from Eq.4 is 0.05 for a beam with a radius of 5 and an image distance of 100. The mean ratio between LSA and TSA from simulation data was 0.04925 ± 0.00089 – a highly accurate result with a 1.5% deviation from the true value. Analysis of the lens system optimized by the L-BFGS-B method indicated a 130.8% and 131.1% deviation from theoretical value [**6**] in TSA and LSA respectively. The deviations are off by degrees of magnitude, indicating the existence of systematic errors.

The existence of aberrations with an optimised lens indicated limitations in either the simulation or the optimisation process, as seen in Fig. 8b. The simulation can model ray optics to a high level of accuracy but neglects the nature of light as an electromagnetic wave. This assumption implies the simulation is unable to account for the interference effects of an optical system. Hence the TSA and LSA measured from the simulation are inaccurate representations of reality, as it is an incomplete model of the nature of light. The different methods approach the optimisation with different algorithms. For example, the L-BFGS-B method utilises the limited memory BFGS algorithm, a family of iterative methods which optimise by analysis of gradient with curvature information [**9**]. The scipy.optimize.minimize function required bounds for the optimisation process to run for the lens system, to limit the case of non-intercepting rays. Hence boundaries were set to limit the values which the optimized parameters can take. This was a limitation on the results of the optimisation, where the parameters for an aberration-free lens system may not have been included within the boundaries.

V. Conclusion

The simulation demonstrated high performance as a model of ray optical systems, correctly presenting results to a high degree of accuracy. The investigation of spherical aberrations using the simulation demonstrated success to a moderate extent, with the relationship between TSA and LSA described accurately but with an unrealistic representation of real-world optical phenomena. The inconsideration of the wave nature of optics limited the simulation. The system can be further scrutinised by constructing an aberration-free output with an aspheric collimator lens and observing whether the simulation will output a clear focal point.

VI. References

[**1**] Smith, A.M. (2017).*From sight to light : the passage from ancient to modern optics.* Chicago ; London: University Of Chicago Press.

[**2**] Waldrop, M.M. (1990). Hubble Trouble. *Science*, 248(4963), pp.1600–1600. doi:10.1126/science.248.4963.1600-a.

[**3**] Mikš, A. and Novák, P. (2012). Determination of unit normal vectors of aspherical surfaces given unit directional vectors of incoming and outgoing rays: comment. *Journal of the Optical Society of America A*, 29(7), p.1356. doi:10.1364/josaa.29.001356.

[**4**] Steward, G.C. (1926). Aberration Diffraction Effects. *Philosophical Transactions of the Royal Society of London. Series A, Containing Papers of a Mathematical or Physical Character*, 225, 131–198. http://www.jstor.org/stable/91156

[**5**] Nussbaum, A. (1968). *Geometric optics*. Reading, Mass.: Addison.

[**6**] Smith, T. T. (1922). Spherical Aberration in thin lenses. *Scientific Papers of the Bureau of Standards*. 18: 559–584. doi:10.6028/nbsscipaper.127

[**7**] Paterson, C. and Kingham, R (2020). Project A: An Optical Ray Tracer. Imperial College Physics Y2 Computing - Short Ptojects (v2.4.1). Accessed 1 November 2022, https://bb.imperial.ac.uk/bbcswebdav/pid-2526807-dt-content-rid-12847106/courses/14925.202210/Computing/Scripts/Projects/.build/html/Raytrace.html

[**8**] Hosken, R.W. (2007). Circle of least confusion of a spherical reflector. *Applied Optics*, 46(16), p.3107. doi:10.1364/ao.46.003107.

[**9**] Mordecai Avriel (2003). Nonlinear Programming. Courier Corporation.

APPENDIX

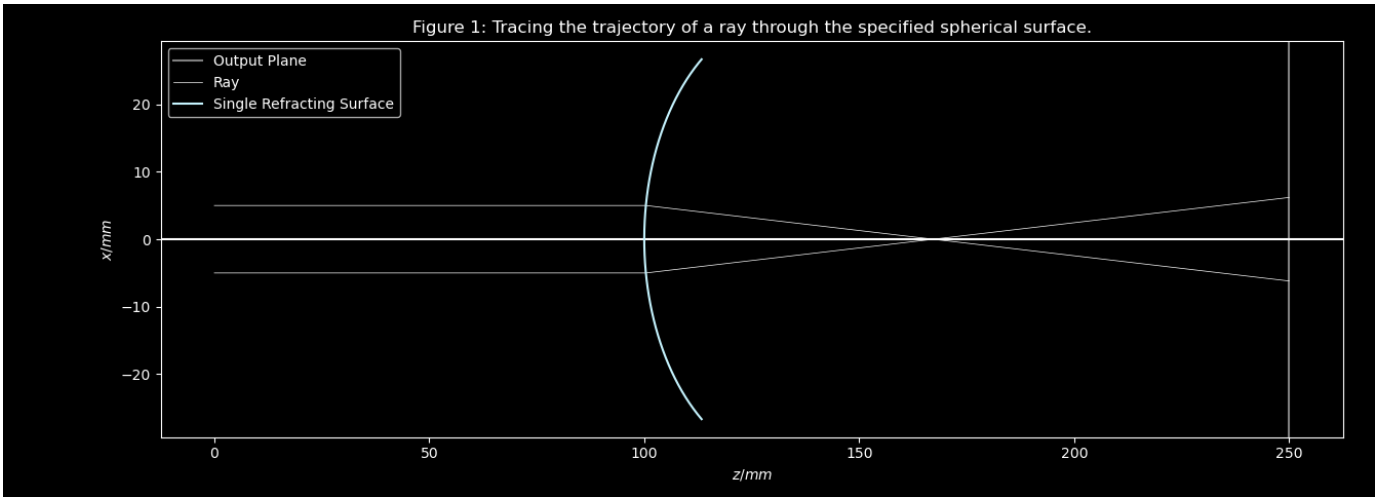
Figure 1: Tracing the trajectory of a ray through the specified spherical surface.
Output Plane
Ray
Single Refracting Surface
x/mm
z/mm

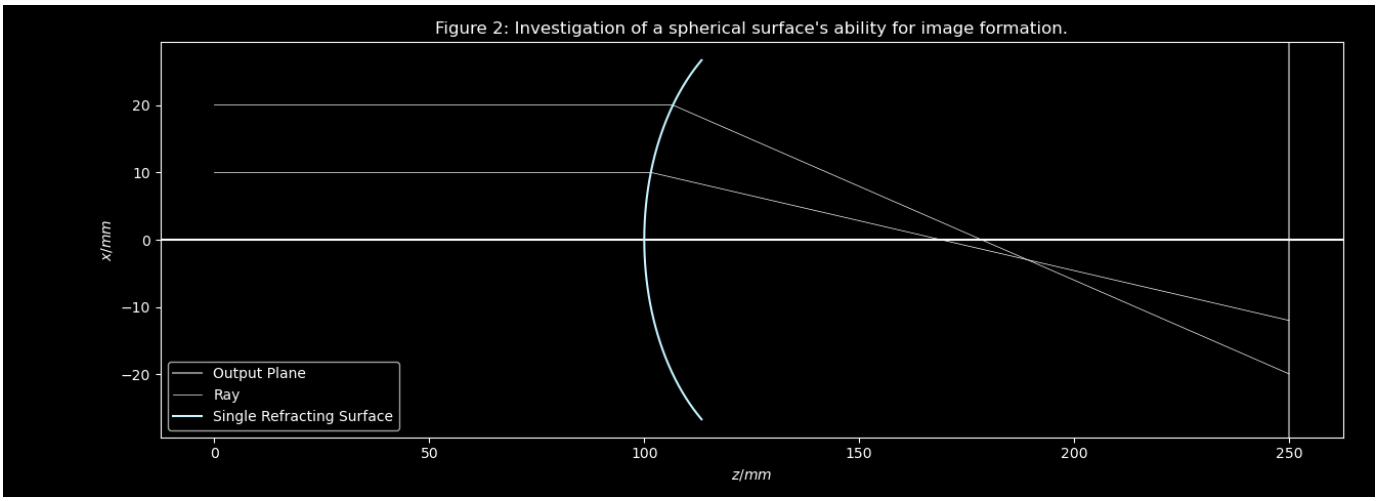
Figure 2: Investigation of a spherical surface's ability for image formation.
Output Plane
Ray
Single Refracting Surface
x/mm
z/mm

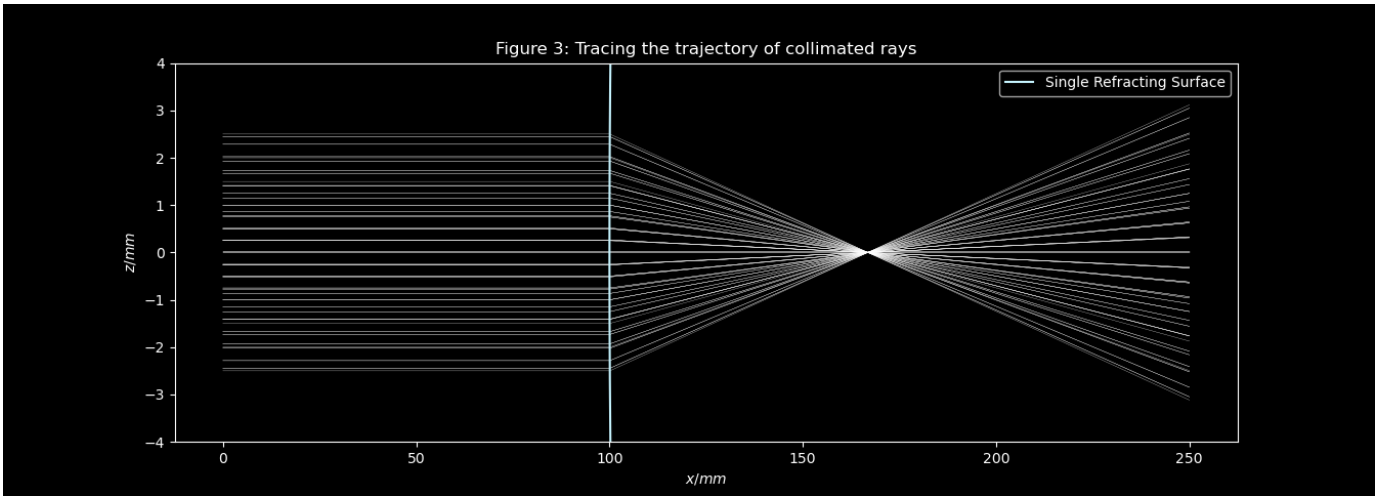
Figure 3: Tracing the trajectory of collimated rays
Single Refracting Surface
z/mm
x/mm

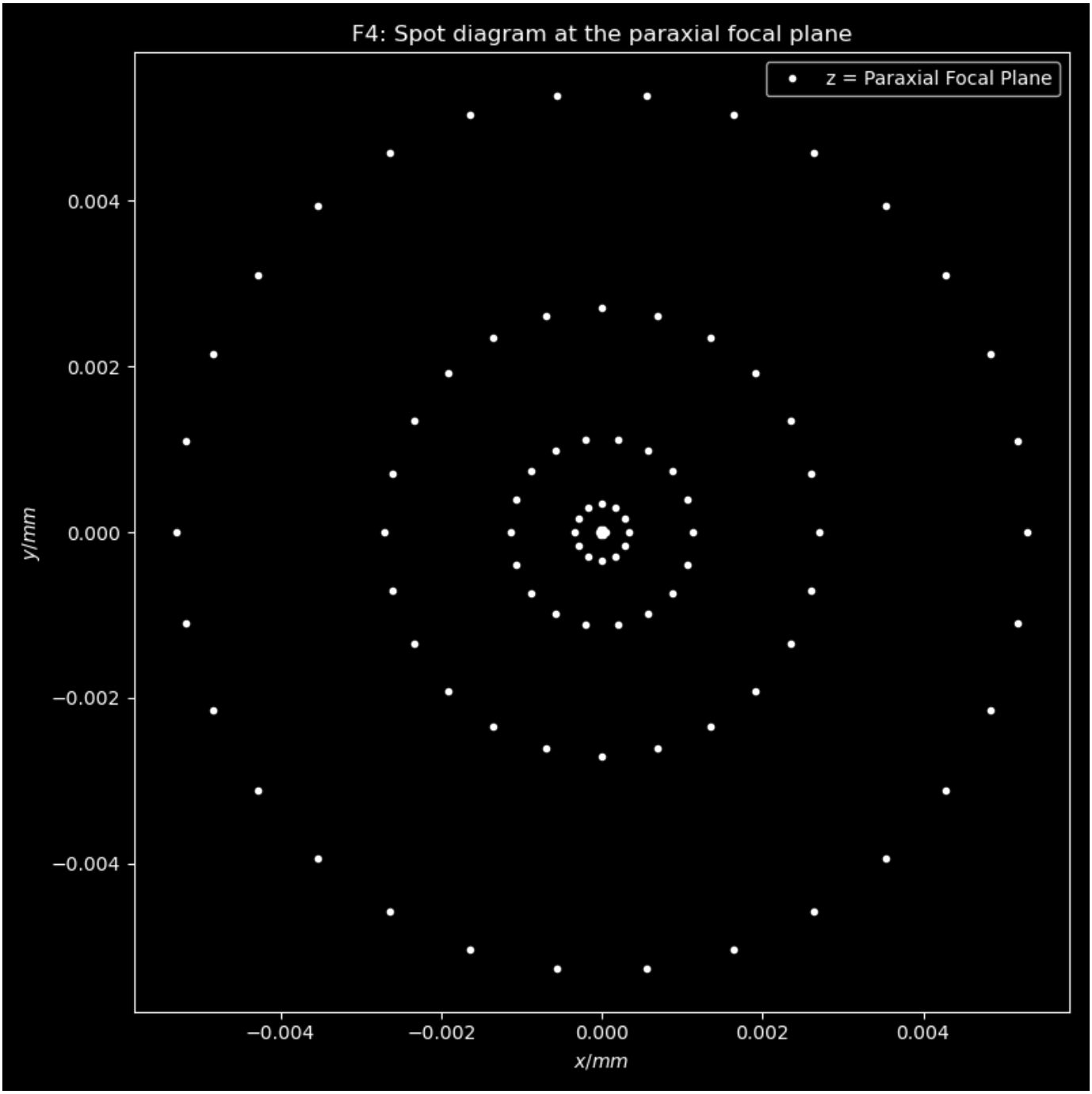
F4: Spot diagram at the paraxial focal plane
z = Paraxial Focal Plane
0.004
0.002
0.000
−0.002
−0.004
y/mm
−0.004
−0.002
0.000
0.002
0.004
x/mm

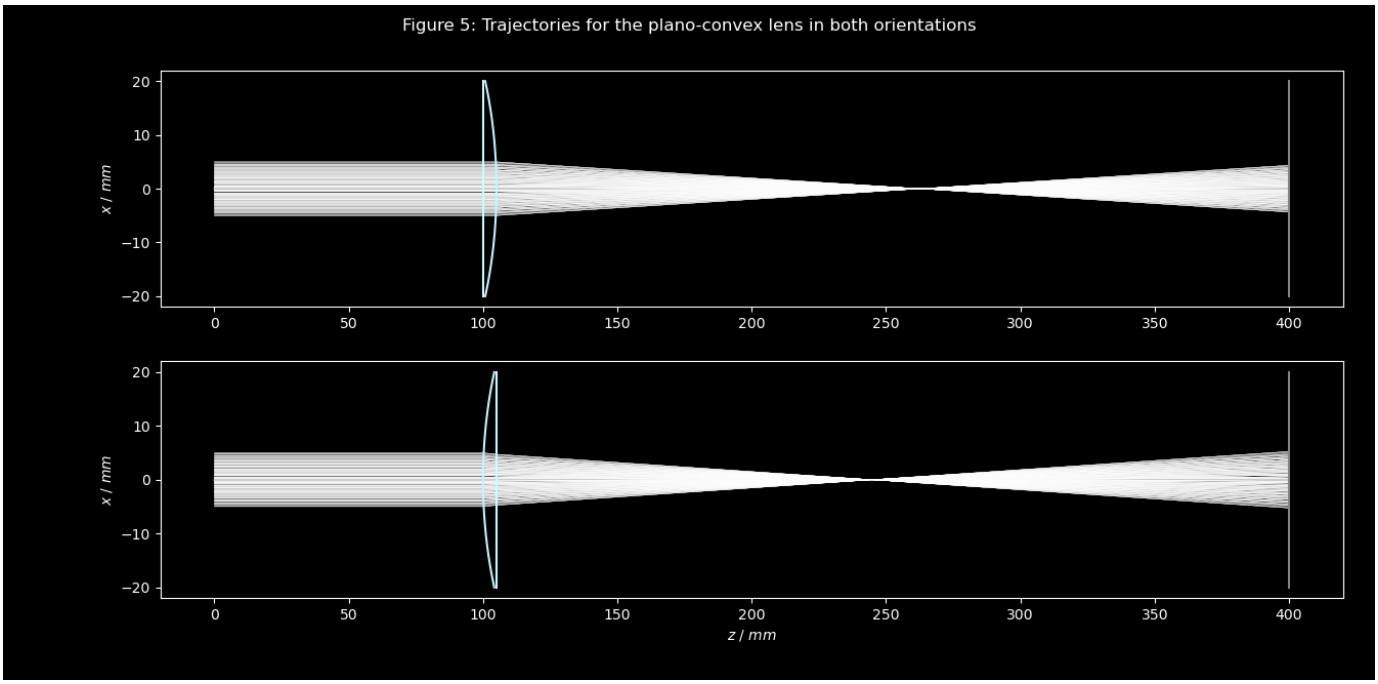
Figure 5: Trajectories for the plano-convex lens in both orientations
x / mm
z / mm

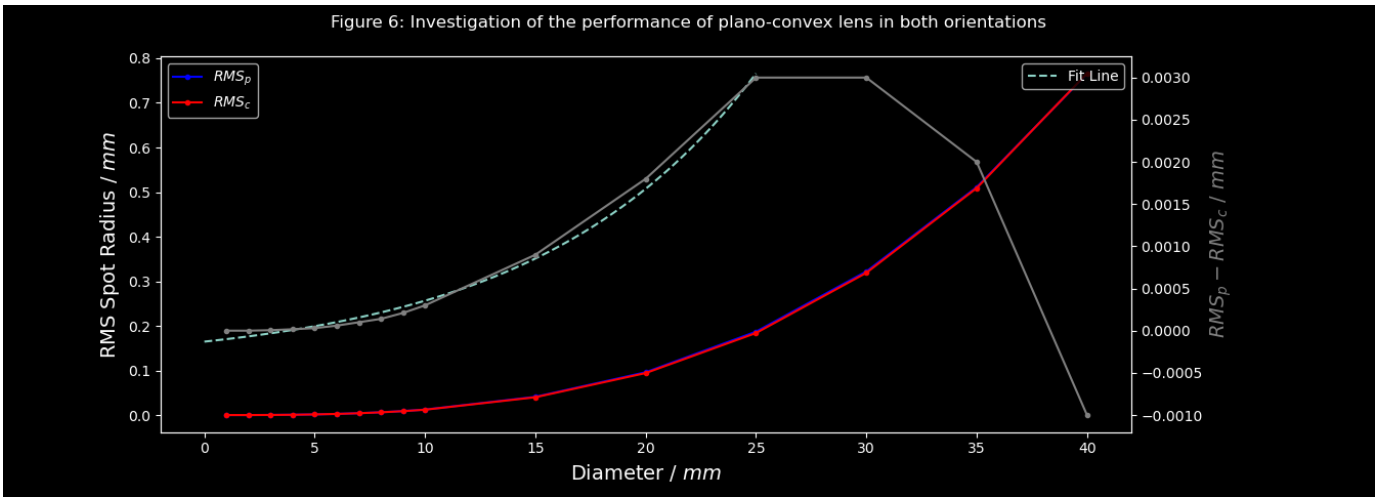
Figure 6: Investigation of the performance of plano-convex lens in both orientations
RMS Spot Radius / mm
Diameter / mm
RMS_p − RMS_c / mm
RMS_p
RMS_c
Fit Line

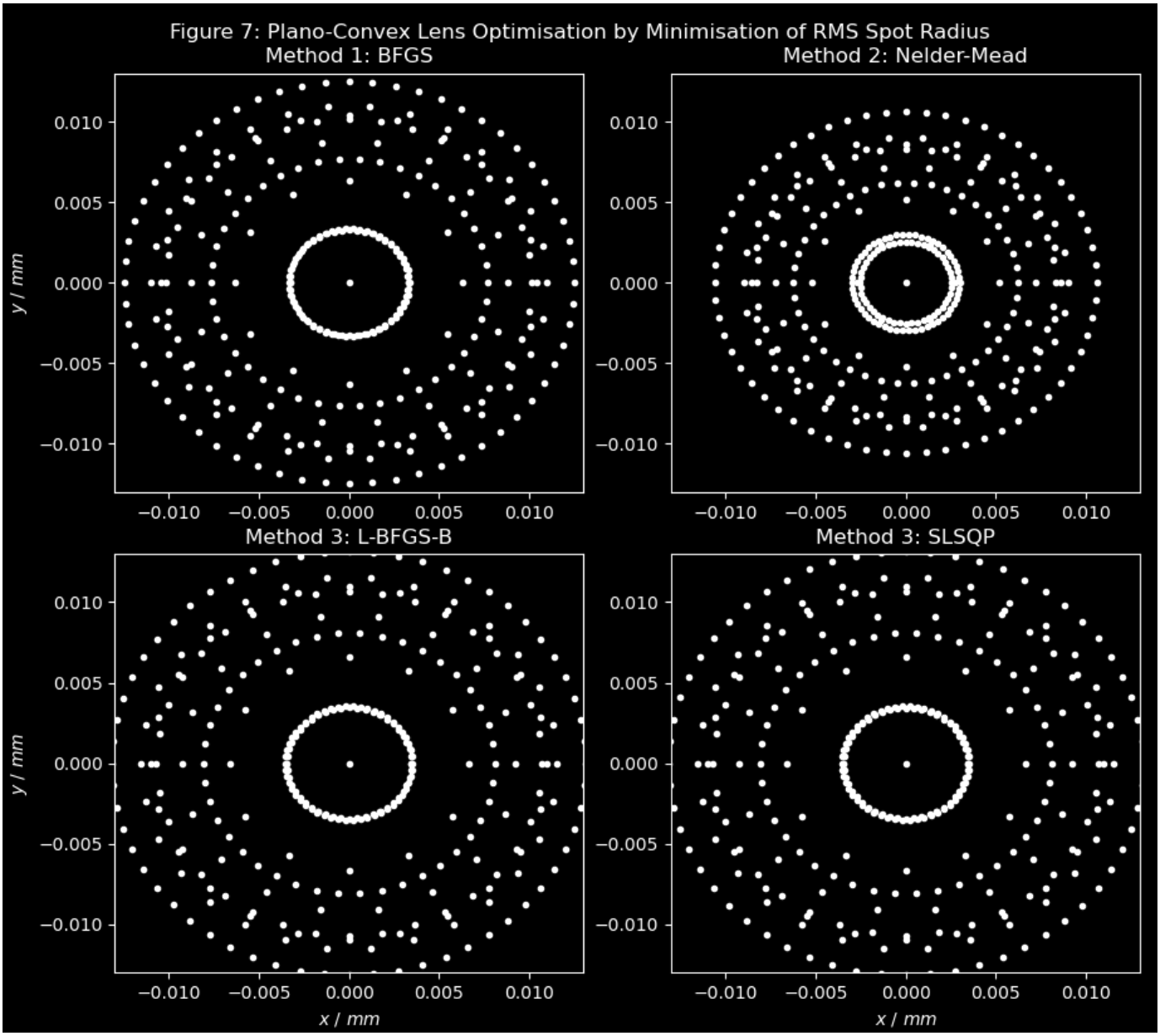
Figure 7: Plano-Convex Lens Optimisation by Minimisation of RMS Spot Radius
Method 1: BFGS
Method 2: Nelder-Mead
Method 3: L-BFGS-B
Method 3: SLSQP
y / mm
x / mm
0.010
0.005
0.000
−0.005
−0.010

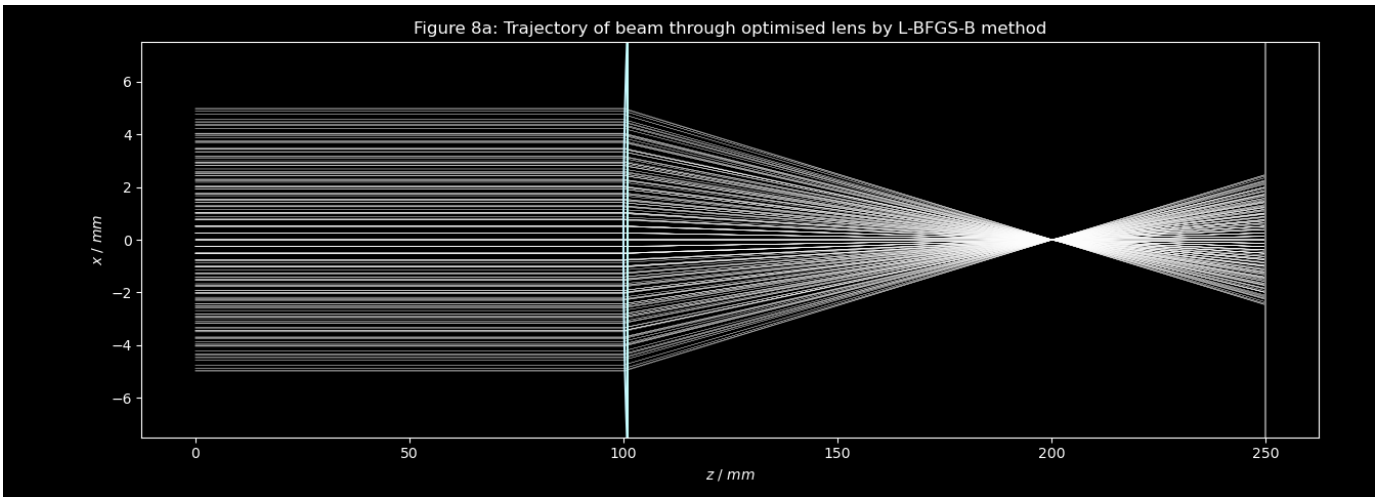
Figure 8a: Trajectory of beam through optimised lens by L-BFGS-B method
x / mm
z / mm
6
4
2
0
−2
−4
−6
0
50
100
150
200
250

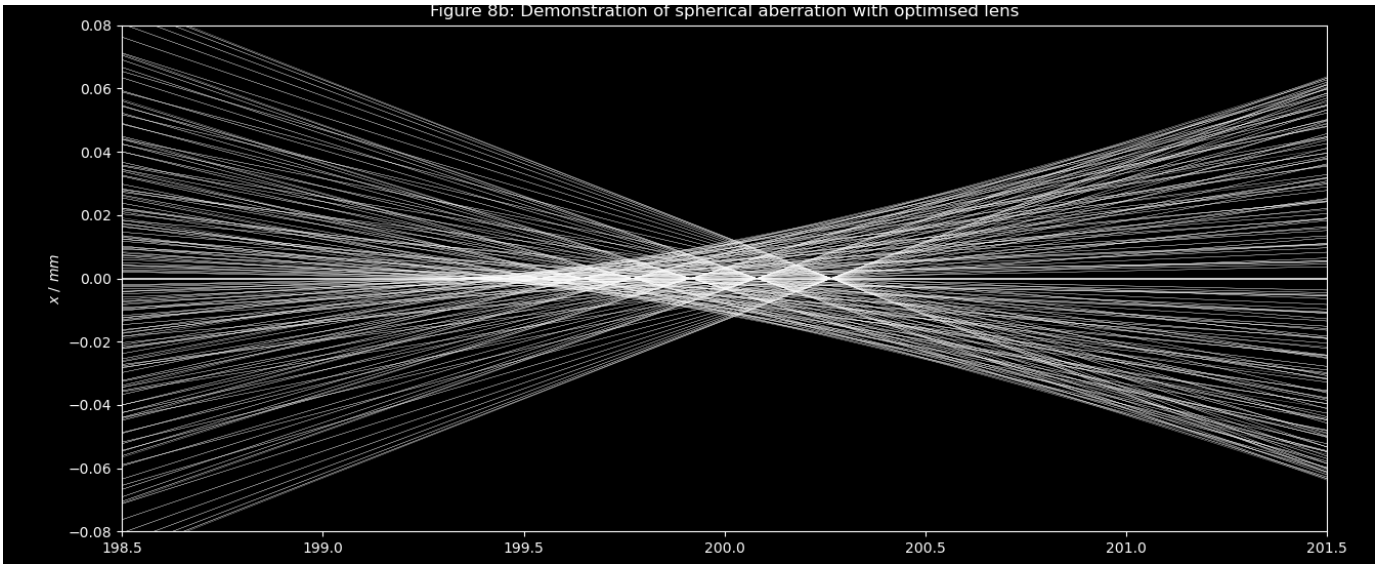

Figure 8b: Demonstration of spherical aberration with optimised lens